ISSN 2278 – 3083

International Journal of Science and Applied Information Technology (IJSAIT), Vol. 4 , No.3, Pages : 43 - 48 (2015)
Special Issue of ICCET 2015 - Held on July 13, 2015 in Hotel Sandesh The Prince, Mysore, India
http://warse.org/IJSAIT/static/pdf/Issue/iccet2015sp06.pdf

Estimation of Energy Dissipation Rate in a Taylor-Couette Reactor using Particle Image Velocimetry

Harminder Singh[1,2], José A. S. Gonçalves[1], Roberto de C. Giordano[1], Claudio A. T. Suazo[1], Alain Liné[2]
[1]Federal University of São Carlos, Brazil, harminder@ufscar.br, jasgon@ufscar.br, roberto@ufscar.br, claudio@ufscar.br
[2]Institut National des Sciences Appliquées, France, line@insa-toulouse.fr

Abstract : A 2D-Particle Image velocimetry (PIV) work in a Taylor-Couette reactor (TCR) is presented on the direct estimate of five of the 12 gradients required for the energy dissipation rate (EDR) estimation at Reynolds number till ~18000 using a 16 Mpixel camera. Special attention was given towards overlap ratio, interrogation cell size (ICS), particle size, time-step and higher order gradients due to their significant impact on the quality of EDR estimation. Viscous EDR was found to be more than 10 times that of the turbulence EDR near the boundary layer, whereas in the bulk zone turbulence EDR is the dominating component of the total EDR. The percentage composition of the five available gradients showed that the tangential velocity gradient in the radial direction accounted for more than 80 % of the viscous EDR in the boundary layer.

Key words: Energy dissipation rate, Hydrodynamics, Particle Image Velocimetry, Taylor-Couette Reactor.

INTRODUCTION

Since early sixties, experimental methods have been shedding light on the flow structures and hydrodynamics in different fluid-flow configurations. In the early eighties and nineties, Smith and Townsend [1] and Kobayashi et al. [2] presented detailed experimental results of the mean and fluctuating velocities for a Taylor-Couette reactor (TCR) using Pitot tubes and hot-wire anemometers. The biggest disadvantage of using these equipment was their intrusive nature and limited data in the boundary layers or near the walls. Although, in recent years computational fluid dynamics has become a more important tool for investigation, the experimental methods are still necessary in order to validate these numerical results. Mavros [3] stated that among the various experimental techniques that are being practiced in recent years for flow visualization and analyzing hydrodynamics, particle image velocimetry (PIV) and laser-Doppler anemometry have become the predominant methods due to their relative easy-to-use techniques and non-intrusive nature. In the case of TCR, PIV has been the primarily used method ([4], [5], [6], [7], [8], [9]) to examine principally the velocity and vortex structures.

Van hout and Katz [10] and Tokgoz et al. [11] presented turbulence parameters, such as Reynolds stresses and energy dissipation rate (EDR), using the PIV method, but their spatial resolution was limited for turbulent Reynolds number. Due to limited spatial resolution, ranging from five to nine time the Kolmogorov scale, Van hout and Katz [10] observed severe underestimation as much as 55 % of the dissipation rate presuming isotropy. Tokgoz et al. [11] found that their tomographic PIV underestimated the mean dissipation, when comparing the PIV estimates with that of torque scaling, by 47% and 97% for shear Reynolds number of 3800 and higher values, respectively. They worked with the spatial resolutions between 3 to 71 times that of Kolmogorov scale, thus also showing the importance of spatial resolution on the estimations of EDR.

Delafosse et al. [12] showed that the spatial resolution plays a strong influence on the estimation of EDR when using the PIV technique. They presented a study of 12 spatial resolutions ranging between one to 12 times the mean Kolmogorov scale, and confirmed that the spatial resolution equal to that of the Kolmogorov scale is required to accurately estimate the EDR. However, they were able to achieve spatial resolution equivalent of Kolmogorov scale at their lowest rotational speed of 50 rpm equivalent of 13 000 Re number. They also observed that when they halved their spatial resolution, the estimation of EDR increased by 220%, in close agreement with the results of Baldi and Yianneskis [13].

Reaching a certain value of spatial resolution depends directly upon the chosen interrogation cell size (ICS) and overlap ratio, apart from the camera and lens equipment. Tokgoz et al. [11] showed improvement in the estimation of EDR with each decrease in the ICS, and increase in the overlap value at a particular ICS. However, there are various other factors, such as time-step between the double framed image, particle size and concentration, and higher orders of the first derivative to estimate the gradients of the velocity vectors, which may also impact the EDR. These aspects, as per author's knowledge, have not been presented.

Secondary problem with the PIV studies is that the spatial resolutions available for 3D is bigger compared to the 2D PIV studies. However, 2D PIV suffers from another limitation apart from the spatial resolution. For a direct estimation of EDR from its equation [14], 12 gradients are required to be calculated, all of which can be estimated with a 3D PIV methods at the expense of spatial resolution; though, only five gradients can be estimated with the 2D PIV method. Due to this limitation, the rest of the seven gradients are required to be estimated based on the isotropic turbulence assumptions [14].

The objective of this study is to present a direct estimate of EDR using a 2D PIV method, thereby presenting only five of the 12 gradients of the equation of EDR. The 2D PIV method is used in order to capture the lowest possible spatial resolution with a 16 M pixel camera. A study will also be conducted to better understand the influence of not only the overlap ratio and ICS but also the time-step, particle size and concentration, and higher order gradients on the EDR estimation.

ISSN 2278 – 3083

International Journal of Science and Applied Information Technology (IJSAIT), Vol. 4 , No.3, Pages : 43 - 48 (2015)
Special Issue of ICCET 2015 - Held on July 13, 2015 in Hotel Sandesh The Prince, Mysore, India
http://warse.org/IJSAIT/static/pdf/Issue/iccet2015sp06.pdf

MATERIALS AND METHODS

Description of case set-up

A TCR, as shown in Fig. 1, with inner, r_i, and outer, r_o, cylinder radius of 100 and 115 mm, respectively, and a height, h, of 200 mm was used in this study. This leads to a gap width, b, radius ratio, η, and aspect ratio, Γ, of 15 mm, 0.87 and 13.3, respectively. Rotational speed, ω, of 114 rpm is used in this study with the Reynolds number, $(r_i\omega(r_o-r_i))/\nu$, and Taylor number, $(r_i^{1/2}\omega(r_o-r_i)^{3/2}/\nu$, of 17900 and 6935, respectively. Inner cylinder was placed at 0 mm above the outer cylinder. Water at room temperature was used as the working fluid.

PIV set-up

The PIV system consists of a class IV Quantel Big Sky Laser (15 Hz and λ=532 nm), FlowSense EO 16 MPixel camera (4872×3248) provided by Dantec Dynamics using a 60mm objective having a diaphragm aperture of f/2.8 to f/32 and a synchronization system, shown in Fig. 1. Silver coated glass beads of 10 µm size were used as seeding particles. The acquired data was processed with an image acquisition system provided by Dantec Dynamics, Dynamicstudio V4.0. The vector analysis was conducted using the adaptive correlation with overlapping windows ranging from 0 to75% and ICS ranging from 64 to 8 pixels squared for high resolution. The spurious vectors were removed using range validation, and then these were replaced by moving average validation using 3 or 5 neighboring cells, in most cases 3 neighboring cells were used.

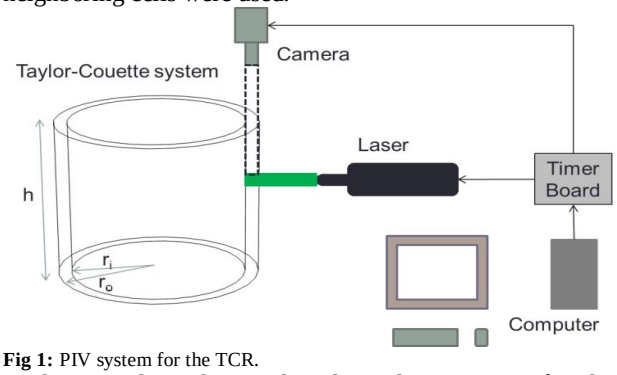

Fig 1: PIV system for the TCR.

The spatial resolutions based on these aspects for the horizontal plan located at $Z_h = 0.725 \pm 0.005$ are presented in the Table 1. A total of 2500 image pairs were found to be more than sufficient for each ω at five different horizontal locations to achieve the statistical convergence of the second order fluctuating velocity components, namely $u_r'^2$, $u_\theta'^2$ and $u_r'u_\theta'$. The five horizontal locations are between $Z_h = 0.525 \pm 0.005$ and 0.725 ± 0.005 with each approx. 10 mm apart from one another.

Table 1: Different ICS and overlap ratios tested.

ICS	Overlap, %	Spatial resolution, µm
64	0	546
32	0	273
	25	205
	50	136
	75	68
16	0	136
	25	102
	50	68
	75	34
8	0	68

Estimation of EDR

The Dantec Dynamic program Dynamicstudio V3.31 was used to process the image pairs to obtain instantaneous velocity profiles. These were extracted as .txt files which were then processed further using Matlab to acquire mean and fluctuating profiles of radial and tangential velocity components, and the EDR. Only five out of 12 gradients for the viscous, ε_ν, and turbulence, ε_τ, EDR are available for a 2D-PIV leading to the Equations 1 and 2, respectively. The PIV measurements were taken in a horizontal plan in a location where U or u' represents mean and fluctuating tangential components and V or v' represents mean and fluctuating radial component of the velocity, and x and y implies tangential and radial directions, respectively, and ν is the kinematic viscosity. The gradients used in the Equations 1 and 2 were estimated using a 2nd, 4th and 6th order central differencing approximation of the first derivative for the central elements, and 2nd, 4th and 6th order forward and backward differencing approximations for the boundary elements, respectively.

$$\varepsilon_\nu = \upsilon\left[2\left(\left(\partial\overline{U}/\partial x\right)^2 + \left(\partial\overline{V}/\partial y\right)^2\right) + \left(\partial\overline{U}/\partial y\right)^2 + \left(\partial\overline{V}/\partial x\right)^2 + 2\,\partial\overline{U}/\partial y \cdot \partial\overline{V}/\partial x\right] \quad (1)$$

$$\varepsilon_\tau = \upsilon\left[2\left(\overline{\left(\partial u'/\partial x\right)^2} + \overline{\left(\partial v'/\partial y\right)^2}\right) + \overline{\left(\partial u'/\partial y\right)^2} + \overline{\left(\partial v'/\partial x\right)^2} + 2\cdot\overline{\partial u'/\partial y \cdot \partial v'/\partial x}\right] \quad (2)$$

RESULTS AND DISCUSSION

Basic Aspects of PIV

Every basic choice in the utilization of PIV equipment has a significant impact on the estimation of the finer quantities, such as EDR. To estimate accurately the smaller structures a very fine spatial resolution is required. The interesting aspect is that the actual spatial resolution is known after the treatment of data, meaning that the concentration of particles, size of particles and time-step between frames is decided by hit and trail method. In addition, all these basic aspects are inter-related to each other. This section shows the importance of these basic aspects in the estimation of the EDR. All these aspects were studied with the 114 rpm rotational speed unless otherwise stated.

A. Size of particles

Fig. 2 presents the influence of particle size on the tangential mean velocity components and its squared fluctuating velocity component located at $Z_h = 0.725 \pm 0.005$ using a time-step of 75 µs. Clearly the reduced particle size has not only improved the tangential mean velocity component but also has a significant impact on its squared fluctuating counterpart. Though there could be a slight difference of ± 1 mm between the two particle size estimations, a probable reason behind slightly different profile structures. Anyhow, in terms of the mean tangential velocity component, the estimations of the 10 µm particle size were completely identical for all four of the ICS values; whereas, for the 20 µm particle size the structures for the four ICS values had some slight differences and a little bit of noise as well. The noise becomes more pronounced for the 20 µm particle size in the estimation of the squared fluctuating

International Journal of Science and Applied Information Technology (IJSAIT), Vol. 4 , No.3, Pages : 43 - 48 (2015)
Special Issue of ICCET 2015 - Held on July 13, 2015 in Hotel Sandesh The Prince, Mysore, India
http://warse.org/IJSAIT/static/pdf/Issue/iccet2015sp06.pdf

tangential velocity component in addition to another problem of doubling of the magnitude with each decrease in the ICS value. In other words, the magnitude increases two times when the ICS value is decreased from 64 to 32 and from 32 to 16 and so on. This increase is not practical, which lead to this study of understanding the influence of particle size on the flow.

Size of particle is important in order to attain the optimum concentration to attain a fine spatial resolution. The smallest available true spatial resolution that is the one with overlap zero is 16 square grid of 136 µm (Table 1). An important point to note is that the 8 grid structure is actually adapted from the 16 grid structure; therefore, 16 square grid is considered as the smallest true spatial resolution available in this study. As per general guidelines, around 5 particles per square grid are considered an optimum concentration. Fitting five particles of the size of 20 µm in grid size of 136 µm is practically very difficult and may result in agglomeration of particles which will hinder further the estimation of smaller scales. Hence, based on this understanding the particle size was reduced from 20 µm to 10 µm, and a drastic improvement was seen in the estimations of squared fluctuating tangential velocity component (Fig. 3b).

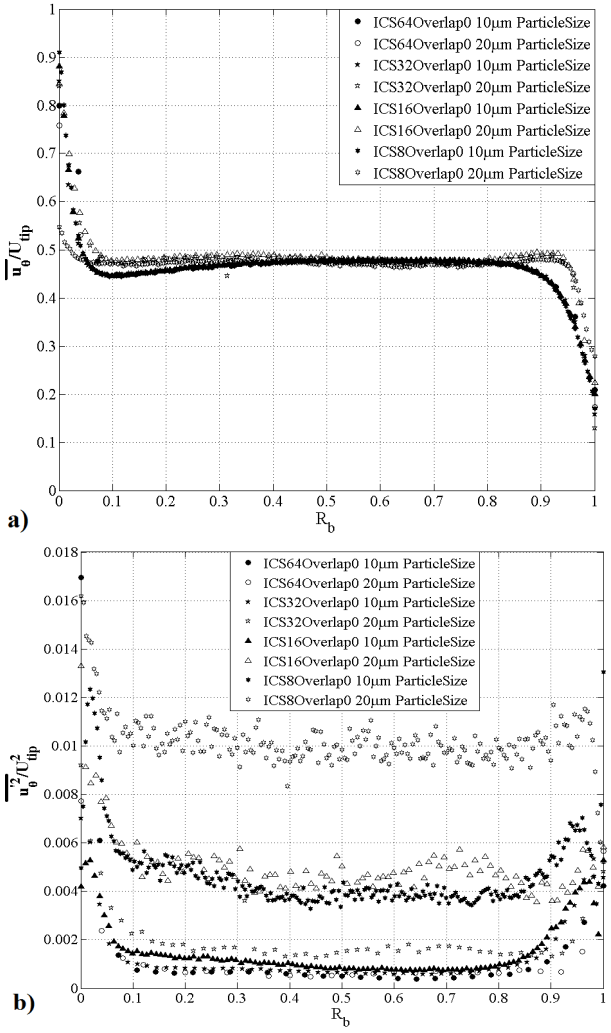

Fig 2: Impact of particle size on the estimations of mean tangential velocity (a) and squared fluctuating velocity (b), where $R_b=r_i/b$.

It can be seen that the magnitude variation between the 64, 32 and 16 square grids is very small with only slight improvements in magnitude and increase in the total number of data points. Moreover, there was very little noise in the data which in comparison to the estimations of the 20 µm is practically unnoticeable. The results of the ICS 8 square grid for the 10 µm particle size were considered unpractical in similarity with the results of the 32, 16 and 8 square grid for the 20 µm particle size. The 8 square grid has a spatial resolution of 68 µm, which implies that fitting five particles of 10 µm size in 68 µm will be a challenging proposition as in the case of the 20 µm particle size. Particles of size of about 2-3 µm are required in order to achieve correct estimations for the 68 µm spatial resolution. However, due to limited time and financial resources it was not possible to use extremely costly particles of mean diameter of 2-3 µm.

B. Time-step between frames

First of all, time-step is the difference in the time between a double frame image capturing the movement of particles within that time-step from the first frame to the second. Depending on the fluid flow conditions and the chosen spatial resolution, the time-step should be small enough to capture the movement of particle from the first frame to the second. As per general guidelines, the movement of particle covering $1/4^{th}$ of the ICS is considered sufficient. However, when the time-step is very small of the order of 100 µs, it becomes necessary to choose time-step wisely. In this case, we studied four different time-steps within the range of 50 to 200 µs.

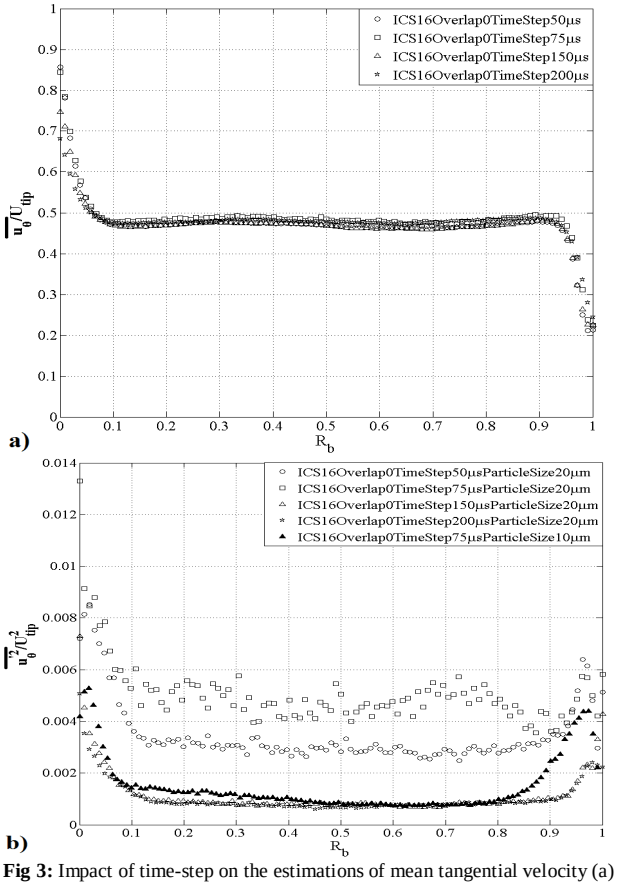

Fig 3: Impact of time-step on the estimations of mean tangential velocity (a) and squared fluctuating velocity (b).

ISSN 2278 – 3083

International Journal of Science and Applied Information Technology (IJSAIT), Vol. 4 , No.3, Pages : 43 - 48 (2015)
Special Issue of ICCET 2015 - Held on July 13, 2015 in Hotel Sandesh The Prince, Mysore, India
http://warse.org/IJSAIT/static/pdf/Issue/iccet2015sp06.pdf

In the Fig. 3, the influence of the time-step on the mean tangential velocity and squared fluctuating velocity component is shown. As in the case of the particle size, there is practically no influence of the time-step on the mean tangential velocity component. On the other hand, in the case of squared fluctuating tangential velocity component, the impact is significant on both the noise and magnitude value. With each decrease in the time-step from 50 towards 150 µs, the noise is reduced drastically and so does the magnitude. The results for the 150 and 200 µs are very similar with little noise.

These estimates of four different time-steps conducted with the 20 µm particle size were compared with the particle size of 10 µm using time-step of 75 µs, to compare with the better estimates of the 10 µm particles. The estimations of the 10 µm particles were found to be very similar with the one using 150 µs time-step for the 20 µm particles. This suggests that the size of particle also plays a significant role in the determination of the time-step. The time-step size for the 20 µm particles is double that for the 10 µm particles to obtain similar results. It should be noted that the slight variation in the profile structure is most probably due to difference of ± 1mm between the profile structures for the two different particle sizes.

To study further this effect of the particle size on the time-step, Fig. 4 presents the estimations of the dimensionless EDR for the two particles sizes located at Z_h = 0.725 ± 0.005. In the x and y axis of the Fig., the shear velocity, u_τ, and ε_{wall} are estimated numerically from the torque estimations of the DNS model, as follows: $u_\tau = (\tau/(\rho V))^{0.5}$, and $\varepsilon_{wall}=u_\tau^4/\nu$. The numerical estimations are used here due to unavailability of the experimental torque estimations in this case.

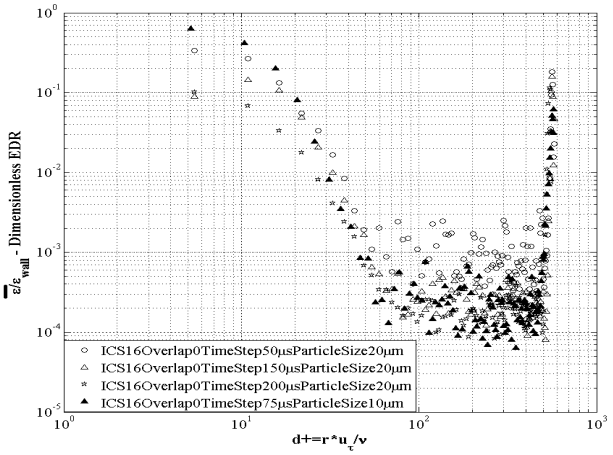

Fig 4: Influence of the time-step and particle size on the viscous EDR.

It can be seen that smaller the time-step is, higher the estimation of the EDR becomes in the case of 20 µm particles. It has been seen that at the 50 µs time-step, the squared fluctuating tangential velocity estimations were unpractical, and these estimations for the 150 and 200 µs time-step were similar. However, this is not the case for the estimation of the EDR where the 150 µ time-step estimations are higher in magnitude in comparison to those of the 200 µs time-step. On the other hand, the estimations of the 10 µm particles at 75 µs time-step are even better in the boundary layer area of the inner cylinder. This clearly demonstrates the need of the smaller time-step and particle size for improved predictions of not only the fluctuating velocity components but also the EDR; thus, making the 10 µm particle size as the preferred choice for this study and 75 µs time-step for the 114 rpm rotational speed.

C. Higher order gradients of the first derivative

Fig. 5 presents the estimations of the three orders, 2nd, 4th and 6th on the EDR at a fixed ICS of 16 square grid and overlap ratio of 0. It can be seen that the major impact of the variation in the gradients is on the bulk region, between d+ = 50 to 500, along with a slight impact in the viscous region, between d+ = 1 to 10. The slight impact in the viscous sub-layer shows the positives of using the higher order terms of the Taylor's expansion, i.e., capturing of more information. On the other hand, the biggest impact which lies in the bulk zone is negative in the sense that with each increase in the order, there is substantial increase in the amount of noise in the small magnitude values present in the bulk zone. Finding a mix between less noise and capturing of more information, leads to the choice of using the 4th order gradients.

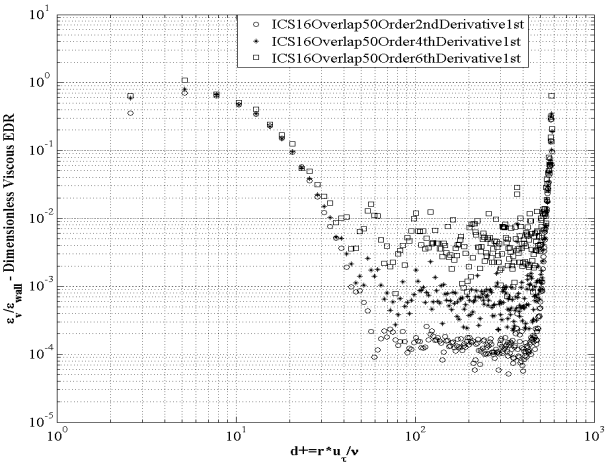

Fig 5: Influence of the higher order gradients of the first derivative on the viscous EDR**.**

D. Overlap ratio

Fig. 6 and 7 present the squared fluctuating tangential velocity and EDR at different overlap ratios for a fixed ICS. It can be seen that practically any overlap value can be chosen for estimating squared fluctuating tangential velocity, or eventually kinetic energy. In agreement with Tokgoz et al. [11], an increment in the overlap value predicts an increase in the EDR (Fig. 7a and 7b); though, at the expense of increased noise. In order to understand this, it becomes important to understand what an overlap is and its function.

An overlap of zero implies that no adjacent interrogation areas were used when velocity vectors were calculated, so the basic objective of overlap is to increase the data yield. Higher the overlap value, smaller the spatial resolution becomes; therefore, we see a spatial resolution of 68 µm at 32, 16 and 8 ICS with an overlap of 75, 50 and 0 respectively, as shown in the Table 1. The overlap window of 75 has too much noise and zero has very few points in the boundary layer. As 50 has been suggested by Dantec dynamics as the suitable overlap value, in addition to less noise in comparison to overlap window of 75 while presenting similar structure as that of 75

International Journal of Science and Applied Information Technology (IJSAIT), Vol. 4 , No.3, Pages : 43 - 48 (2015)
Special Issue of ICCET 2015 - Held on July 13, 2015 in Hotel Sandesh The Prince, Mysore, India
http://warse.org/IJSAIT/static/pdf/Issue/iccet2015sp06.pdf

overlap window, it has been chosen as the overlap value for all of the results represented from now-onwards.

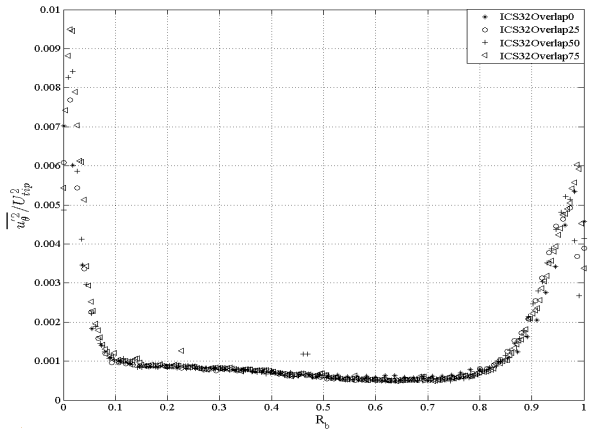

Fig 6: Radial profile squared fluctuating tangential velocity at different overlap ratios.

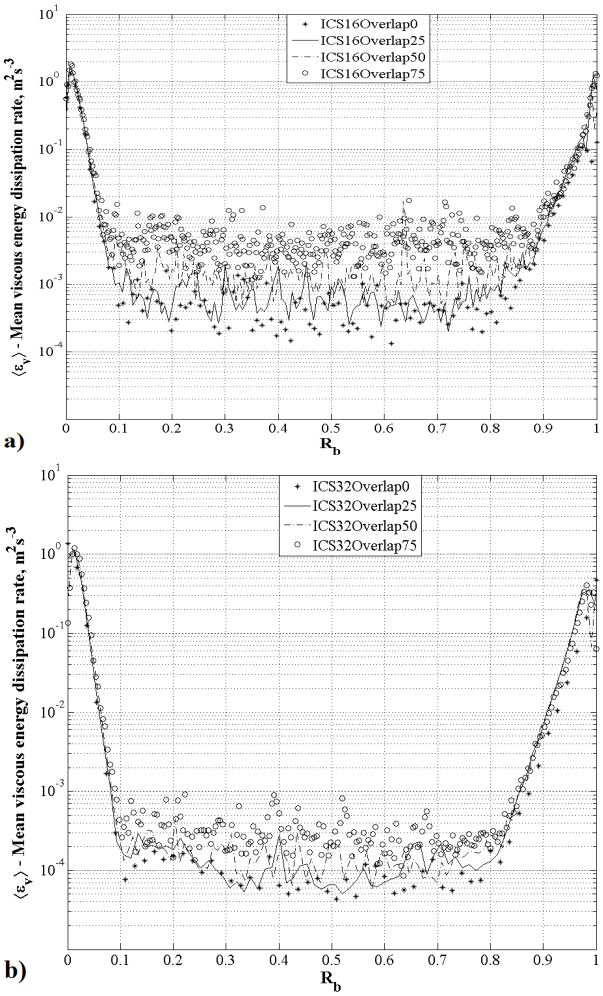

Fig 7: Radial profile of mean energy dissipation rate at ICS value of 16, a), and 32, b), with each at different overlap values.

E. ICS

Fig. 2a shows that the mean tangential velocity profile becomes independent of the ICS from 32 pixels squared onwards or 273 µm; in other words, at higher ICS values the flow structure may not be the actual representation. Whereas, the estimation of the squared fluctuating tangential velocity shows that 16 pixels squared presents the best prediction (Fig. 2b), considering the estimates of the 8 square grid to be unpractical as explained earlier. In addition, in Fig. 7a and 7b, it can be seen that there is a difference of an order in the bulk zone in the estimation of EDR at 16 and 32 ICS. Therefore, 16 square grid has been chosen for the rotational velocity of 114 rpm due to better estimation of EDR both in the boundary layer and bulk zone.

Energy Dissipation Rate

A. Viscous and turbulence EDR

The two components of the total EDR, viscous and turbulence are presented in Fig. 8. The two EDR components, viscous and turbulence have the maximas on the walls then the magnitude decreases towards the middle of the gap-width. The decrease for both these components is steep in the boundary layer, though it should be noted that the magnitude of the viscous component is around an order higher than the turbulence component in this region. In the bulk region, the turbulence EDR is comparatively higher. This shows that the viscous force is the predominant force in the boundary layer area; while, turbulence is stronger of the two in the bulk zone.

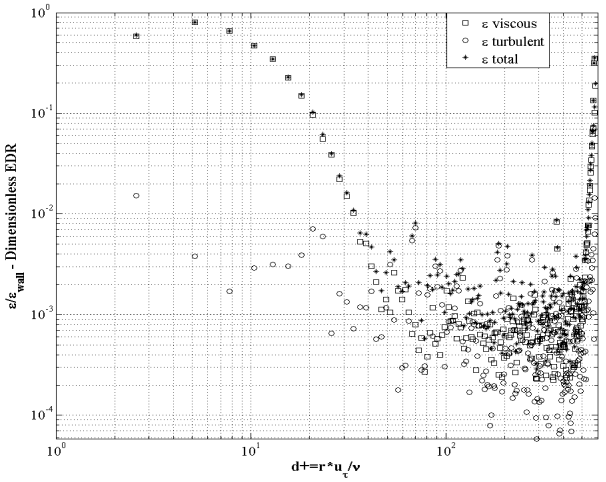

Fig 8: Division of the total EDR in the viscous and turbulent components.

Moreover, it can be seen that the viscous EDR is moving towards unity when d+ approaches 5, and the ratio remains almost constant in the viscous sublayer between 1<d+<5. As d+ tends towards 40, a steep decrease in the viscous EDR can be observed and the turbulence EDR becomes stronger than the viscous EDR. Furthermore, the turbulence EDR behaves as d+ power minus one between the 10< d+ < 20 region. These aspects of following the classical turbulence clearly demonstrate the validity of these results.

B. Percentage composition of EDR

In the Fig. 9, the percentage composition of each of the five gradients of EDR estimation is presented. It can be clearly seen that in the boundary layer area more than 50% alone is represented by only $(\partial U/\partial y)^2$ gradient, where U and y implies tangential velocity and radial direction, respectively. In other words, capturing the propagation of tangential velocity in the

International Journal of Science and Applied Information Technology (IJSAIT), Vol. 4 , No.3, Pages : 43 - 48 (2015)
Special Issue of ICCET 2015 - Held on July 13, 2015 in Hotel Sandesh The Prince, Mysore, India
http://warse.org/IJSAIT/static/pdf/Issue/iccet2015sp06.pdf

radial direction is of utmost importance in order to estimate well the EDR in the boundary layer. In the bulk zone, on the contrary, the contribution of all gradients is very similar. However, as seen earlier the EDR in the bulk zone is 10 times smaller compared to the magnitude in the boundary layer area. Thereby further enhancing the importance of the $(\partial U/\partial y)^2$ gradient in the estimation of mean EDR. Although, there are only five gradients instead of 12 for the complete estimation of EDR, it is known that the axial velocity is also not very strong in this Taylor-couette flow. The impact of axial flow on the EDR could be considered to be similar to that of the radial flow, i.e. in the bulk zone and very little in the boundary layer.

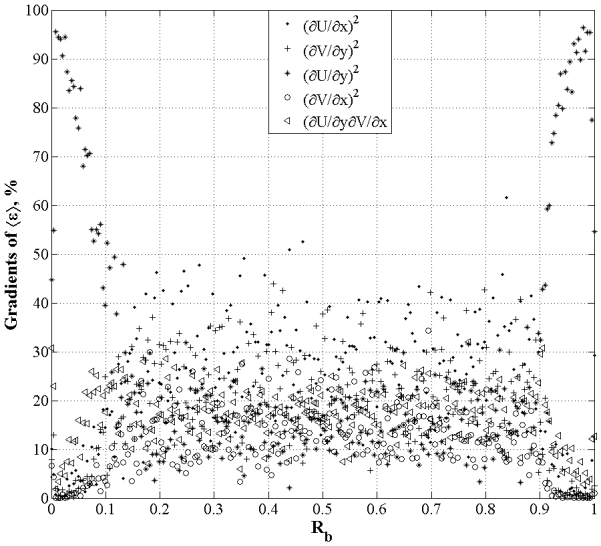

Fig 9: Percentage composition of each of the five gradients in the estimation of viscous EDR.

If isotropic or axi-symmetry assumptions are applied [14] in this case, then it would mean that the $(\partial U/\partial y)2$ gradient would be two or three times, respectively, meaning that the EDR estimation will be a multiple of the $(\partial U/\partial y)2$ gradient. Being a tangential flow, the radial and axial flows are weak, each being only about 10% of the tangential flow [2]; therefore, these assumption based estimations cannot be considered in this case of TCR. For a better estimation, it is important to know the percentage composition of each of the 12 gradients on the EDR, afterwards a newer and simpler equation can be created for 2D PIV results. This can be done with a direct numerical simulation for this configuration because experimentally the estimation of all 12 gradients while capturing the smallest scales is still out of reach as shown by Tokgoz et al. [11].

CONCLUSION

The 2D PIV study presented here showed the significance of all the basic aspects of the PIV in the estimation of EDR. To reach the Kolmogorov scale at turbulent Reynolds number very fine spatial resolution is required which implies that smaller particle size, time-step and ICS are necessary along with the usage of higher order gradients. Overlap ratio's function is to increase the number of data points in the boundary layer but at the expense of increased noise with each increase in the overlap ratio. The maximum of the viscous EDR lies near the wall and is about 1000 times stronger than the one in the bulk zone which comprises 80 % of the reactor space. Additionally, only one gradient, $(\partial U/\partial y)^2$, represents more than 50 % of the viscous EDR in the boundary layer where lies the steepest gradient. In order to estimate EDR and other parameters through-out the reactor, capturing computationally these steep gradients in the boundary layer will require very fine mesh near the walls which can be made comparatively courser towards the center of the gap-width.

ACKNOWLEDGEMENT

This study has become possible due to the postgraduate (processo nº 140756/2012-4) and "Doutorado Sanduíche" (processo numero - 241739/2012-8) Scholarship programs of Conselho Nacional de Desenvolvimento Cientifico e Tecnologico (CNPq), Brasil.

REFERENCES

[1] G. P. Smith and A. A. Townsend, "Turbulent couette flow between concentric cylinders at large Taylor numbers," *Journal of Fluid Mechanics*, vol. 123: pp. 187-217, May 1982..

[2] M. Kobayashi, H. Maekawa, T. Takano and Y. Yamada, "An experimental studyo n turbulent Taylor vortex flow between concentric cylinders," *JSME International Journal II*, vol. 33, no. 3, pp. 436-445, 1990.

[3] P. Mavros, "Flow visualization in stirred vessels: A review of experimental techniques," *Chemical Engineering Research and Design*, vol. 79, pp. 113-127, March 2001.

[4] A. Akonur and R. M. Lueptow, "Three-dimensional velocity field for wavy Taylor-Couette flow," *Physics of Fluids*, vol. 15, no. 4, pp. 947-960, April 2003.

[5] C. Coufort, D. Bouyer, and A. Liné, "Flocculation related to local hydrodynamics in a Taylor–Couette reactor and in a jar," *Chemical Engineering Science*, vol. 60, pp. 2179-2192, Jan. 2005.

[6] R. Deng, D. Y. Arifin, M. Y. Chyn and C. H. Wang, "Taylor vortex flow in presence of internal baffles," *Chemical Engineering Science*, vol. 65: pp. 4598-4605, May 2010.

[7] L. Wang, M. G. Olsen, and R. D. Vigil, "Reappearance of azimuthal waves in turbulent Taylor–Couette flow at large aspect ratio," *Chemical Engineering Science*, vol. 60, no. 20, pp. 5555-5568, June 2005.

[8] S. T. Wereley and R. M. Lueptow, "Spatio-temporal character of non-wavy and wavy Taylor–Couette flow," *Journal of Fluid Mechanics*, vol. 364, pp. 59-80, 1998.

[9] J. Dusting and S. Balabani, "Mixing in a Taylor–Couette reactor in the non-wavy flow regime," *Chemical Engineering Science*, vol. 64, no. 13, pp. 3103-3111, July 2009.

[10] R. van Hout and J. Katz, "Measurements of mean flow and turbulence characteristics in high-Reynolds number counter-rotating Taylor-Couette flow," *Physics of Fluids*, vol. 23, pp. 105102-11, Oct. 2011.

[11] S. Tokgoz, G. E. Elsinga, R. Delfos and J. Westerweel, "Spatial resolution and dissipation rate estimation in Taylor--Couette flow for tomographic PIV," *Experiments in Fluids*, vol. 53, no. 3, pp. 561-583, May 2012.

[12] A. Delafosse, M. L. Collignon, M. Crine and D. Toye, "Estimation of the turbulent kinetic energy dissipation rate from 2D-PIV measurements in a vessel stirred by an axial Mixel TTP impeller," *Chemical Engineering Science*, vol. 66, pp. 1728-1737, Jan. 2011.

[13] Baldi, S. and M. Yianneskis, "On the quantification of energy dissipation in the impeller stream of a stirred vessel from fluctuating velocity gradient measurements," *Chemical Engineering Science*, vol. 59, pp. 2659-2671, May 2004.

[14] Sharp, K.V. and R.J. Adrian, "PIV study of small-scale flow structure around a Rushton turbine,". *American Institute of Chemical Engineers - AIChE*, vol. 47, no. 4, pp. 766-778, April 2001.